

Article

Statistical Analysis of Hybrid Atmospheric Ducts over the Northern South China Sea and Their Influence on Over-the-Horizon Electromagnetic Wave Propagation

Yang Shi ^{1,2} , Shuwen Wang ^{1,2,3,*} , Fan Yang ^{1,2,3} and Kunde Yang ^{1,2,3}

¹ School of Marine Science and Technology, Northwestern Polytechnical University, Xi'an 710072, China; shiyang@nwpu.edu.cn (Y.S.); youngfun@mail.nwpu.edu.cn (F.Y.); ykdzym@nwpu.edu.cn (K.Y.)

² Key Laboratory of Ocean Acoustics and Sensing, Ministry of Industry and Information Technology, Northwestern Polytechnical University, Xi'an 710072, China

³ Ocean Institute, Northwestern Polytechnical University, Taicang 215400, China

* Correspondence: wangshuwen@mail.nwpu.edu.cn

Abstract: Atmospheric ducts are special super-refractive atmospheric structures that can cause over-the-horizon propagation of electromagnetic waves. Different types of atmospheric ducts have different influences on electromagnetic wave propagation. Owing to the complex marine atmospheric environment, different types of atmospheric ducts often occur together. When evaluating the performance of an electromagnetic system near the sea surface, the combined influence of various atmospheric ducts should be considered comprehensively. In this paper, the statistical distribution of atmospheric ducts over the northern South China Sea is analyzed using sounding data and reanalysis data. This paper uses the parabolic equation model to analyze the propagation characteristics of microwaves near the sea surface in the presence of both surface and evaporation ducts. It is found that compared with cases where only one type of atmospheric duct is considered, a hybrid atmospheric duct structure can capture more microwave energy at a lower receiving height. At an antenna height of 5 m, the path loss begins to fluctuate beyond a propagation distance of 50 km, with the maximum fluctuation reaching about 15 dB. Microwave propagation characteristics at different microwave frequencies and antenna heights are also simulated and analyzed.

Keywords: statistical analysis; hybrid atmospheric duct; northern South China Sea; marine time channel; electromagnetic wave propagation



Citation: Shi, Y.; Wang, S.; Yang, F.; Yang, K. Statistical Analysis of Hybrid Atmospheric Ducts over the Northern South China Sea and Their Influence on Over-the-Horizon Electromagnetic Wave Propagation. *J. Mar. Sci. Eng.* **2023**, *11*, 669. <https://doi.org/10.3390/jmse11030669>

Academic Editor: Rouseff Daniel

Received: 14 February 2023

Revised: 9 March 2023

Accepted: 21 March 2023

Published: 22 March 2023



Copyright: © 2023 by the authors. Licensee MDPI, Basel, Switzerland. This article is an open access article distributed under the terms and conditions of the Creative Commons Attribution (CC BY) license (<https://creativecommons.org/licenses/by/4.0/>).

1. Introduction

Atmospheric ducts are special refractive atmospheric structures that form in the troposphere [1–3]. The existence of atmospheric ducts has substantial impacts on the propagation of electromagnetic waves [4–7]. Atmospheric ducts exist widely over the world's oceans. In an atmospheric duct region, electromagnetic waves are refracted toward the sea surface and act as if they are caught in a waveguide. Atmospheric ducts can decrease the path loss of radio wave propagation, and notably affect the operating range of shipborne radar and communication systems.

There are three main kinds of atmospheric ducts: evaporation ducts, surface ducts and elevated ducts. While evaporation ducts are common over many ocean regions, they form due to rapid variations in humidity within the air-sea boundary layer above the sea (usually below 40 m) and their persistence and strength can vary significantly depending on environmental factors such as temperature, humidity, and wind speed. Evaporation ducts are identified as a propagation mechanism that results in substantially stronger signals for over-the-horizon and over-sea paths in the microwave band [5,8–11]. Surface ducts and elevated ducts [12] are usually formed due to the atmospheric temperature inversion layer and decreasing humidity with altitude.

The climatology of atmospheric ducts describes the occurrence probability of the atmospheric ducts and their spatial and temporal variability in the study area. Inhomogeneity and dynamic changes in atmospheric and oceanic factors directly influence the climatology of atmospheric ducts. So far, considerable research has been carried out on the spatial and temporal variability of evaporation ducts in ocean areas of interest, such as the western Pacific Ocean [13], the South China Sea [14–16], the Gulf of Aden [17], and other ocean areas [18–21]. Statistical analyses of the evaporation duct height (EDH) and the spatiotemporal features of evaporation ducts over these areas have been performed in detail using long-term reanalysis datasets. For low-altitude atmospheric ducts, radiosonde sounding data collected in the South China Sea and the East Indian Ocean have been used to analyze the statistical features of surface ducts and elevated ducts [1]. Previous studies of atmospheric duct climatology have usually considered only one type of atmospheric duct. However, hybrid atmospheric ducts (an evaporation duct with a surface duct, or an evaporation duct with an elevated duct) have been found in recent studies [22]. The South China Sea has been the focus of much recent study, but the statistical features of hybrid atmospheric ducts in this area need to be further studied.

The influence of atmospheric ducts on the propagation of electromagnetic waves has been widely studied based on both numerical simulations and field observations. Many numerical models have been used to predict radio wave propagation in atmospheric ducts, including the radio physical optics (RPO) model, the parabolic equation (PE) model [23], and hybrid models [24]. Radio wave propagation in a range-dependent tropospheric environment can be predicted using the PE model. The Advanced Propagation Model (APM) [24] is a hybrid model that combines the RPO model with the PE model. The APM is utilized in the Advanced Refractivity Effects Prediction System (AREPS), which is frequently applied in the assignment of shipborne radio systems. These models have been evaluated in many atmospheric duct experiments, such as the Rough Evaporation Duct experiment [25] and the Coupled Air–Sea Processes and Electromagnetic Ducting Research experiment [26,27]. Moreover, the effects of typhoons [28,29], rainfall [30], and obstacles [31] and the evaporation duct's inhomogeneity [32,33] on radio wave propagation over the South China Sea have been investigated using numerical models and observations. The results have shown that both surface ducts and elevated ducts have considerable impacts on electromagnetic wave propagation above the ocean surface. However, the influence of hybrid atmospheric ducts on electromagnetic wave propagation has seldom been reported.

In this paper, the statistical features of hybrid atmospheric ducts are investigated using long-term radiosonde sounding data and reanalysis data for the northern South China Sea. In addition, the influence of hybrid atmospheric ducts on electromagnetic wave propagation above the ocean surface is presented. The rest of this paper is structured as follows. Section 2 details the data and models used in this paper. In Section 3, the statistical features of hybrid atmospheric ducts over the northern South China Sea are analyzed. In Section 4, the influence of hybrid atmospheric ducts on over-the-horizon electromagnetic wave propagation is presented. In Section 5, the impacts of frequency and antenna height on electromagnetic wave propagation are discussed. Finally, conclusions are presented in Section 6.

2. Data and Methods

Figure 1 shows a flow chart for this study. Radiosonde sounding data collected for two years (2018 and 2019) near Hong Kong in the northern South China Sea were used to analyze surface ducts and elevated ducts. Reanalysis data from the National Centers for Environmental Prediction (NCEP) Climate Forecast System Reanalysis (CFRS) cover the same time period, and the Navy Atmospheric Vertical Surface Layer Model (NAVSLaM) was applied to simulate evaporation duct distribution. The statistical features of hybrid atmospheric ducts in this area were investigated based on the analysis of surface ducts, elevated ducts, and evaporation ducts. Moreover, utilizing the hybrid atmospheric duct

results, the APM model was used to evaluate the influence of hybrid atmospheric ducts on electromagnetic wave propagation beyond visual range.

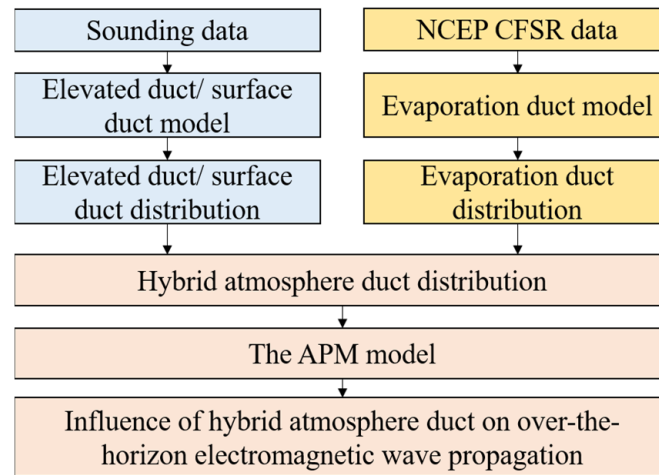


Figure 1. Flow chart for this study.

2.1. Data

2.1.1. Radiosonde Sounding Data

Radiosonde sounding data were used to calculate the distribution of surface ducts and elevated ducts. The sounding data were downloaded from Wyoming Weather Web [34], released by the University of Wyoming. Figure 2 shows the location of the radiosonde sounding station. The station is located near Hong Kong, China (22.31° N, 114.17° E). The station number is 45004. The sounding data are released twice a day, at 00:00Z and 12:00Z. They include air pressure, temperature, dewpoint temperature, relative humidity, wind direction, wind speed, potential temperature, equivalent potential temperature, and virtual potential temperature at different vertical heights. The air pressure, temperature, and relative humidity at different heights were used to simulate the modified refractivity profiles (*M*-profiles) for surface ducts and elevated ducts. Figure 3 shows the meteorological data and the calculated *M*-profile at 12:00 on 27 March 2019 and *M*-profiles for March 2019. The *M*-profiles show that duct occurrences have a negative vertical slope of *M*.

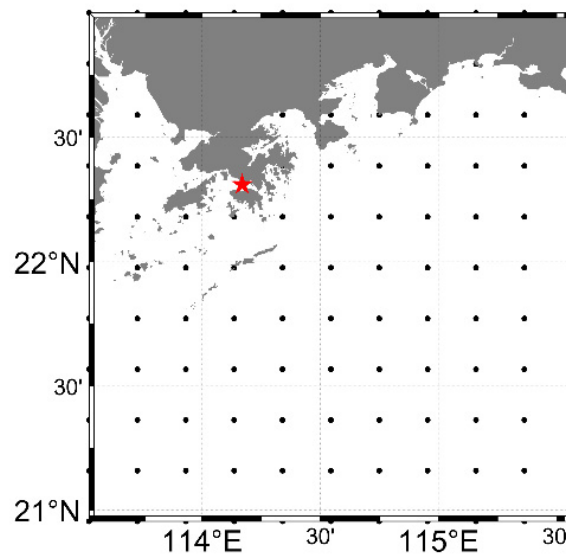


Figure 2. The location of the radiosonde sounding station.

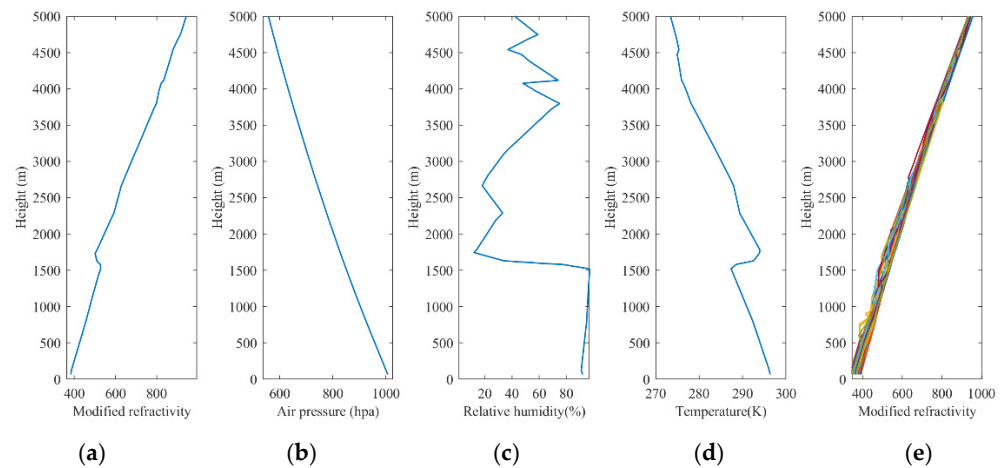


Figure 3. Radiosonde sounding data at 12:00 on 27 March 2019 (a–d) and the *M*-profiles for March 2019 (e).

2.1.2. Reanalysis Data

NCEP Climate Forecast System Version 2 (CFSv2) reanalysis data [35] were applied to predict evaporation duct distribution. The NCEP produces a record of global atmospheric data from numerous sources, including land, surface, ships, radiosonde, aircraft and satellites, through a data assimilation system. NCEP upgraded the climate forecast system to version 2 on 30 March 2011. Beginning with 1 January 2011, the NCEP CFSv2 data are archived as an extension of the CFSR. The spatial coverage of the NCEP CFSv2 is 1760×880 grid points from 0° E to 359.795° E and 89.844° N to 89.844° S, which offers data with a high spatial resolution ($0.205^\circ \times 0.205^\circ$). The temporal resolution is 1 h. Figure 2 shows the grid points of the NCEP CFSv2 data. Table 1 shows the primary atmospheric parameters derived from the reanalysis data and those simulated from the available data.

Table 1. Primary atmospheric variables obtained from the reanalysis data and those calculated from the available data.

| | Parameter | Level | Units |
|----------------------|-------------------------|-------------|-------|
| Reanalysis variables | Air temperature | 2 m | °C |
| | Sea surface temperature | Sea surface | °C |
| | Sea level pressure | Sea surface | hPa |
| | u component of wind | 10 m | m/s |
| | v component of wind | 10 m | m/s |
| | Specific humidity | 1000 hPa | kg/kg |
| Calculated variable | Wind speed | 10 m | m/s |
| | Air-sea temperature | 2 m | °C |
| | Evaporation duct height | / | m |

2.2. Atmospheric Duct Model

The propagation of electromagnetic waves in the troposphere depends on the refractivity index of air, n . Because of differences in air pressure, air temperature, and water vapor concentration, the index of refractivity fluctuates throughout the troposphere. The refractivity index n is specified as the proportion of light speed in a vacuum, c_0 , and the speed of the wave, v . The index of refraction in the troposphere for radio waves is obtained using the Debye theory:

$$n = \frac{c_0}{v} = 1 + \frac{77.6}{T} \times \left(P + \frac{4810e}{T} \right) \times 10^{-6} \tag{1}$$

where T (K) stands for the air temperature, P (hPa) stands for the total air pressure, and e (hPa) stands for the water vapor partial pressure. The water vapor partial pressure e can be determined from the specific humidity using the following equation:

$$e = \frac{qP}{\varepsilon + (1 - \varepsilon)q} \tag{2}$$

where ε is the ratio between the specific gas constants for dry air and water vapor and q (kg kg^{-1}) indicate the specific humidity.

The refractive index in the troposphere fluctuates among 1.000250 and 1.000400 n units. As it is so close to unity, the troposphere’s refractive index is defined by a parameter denoted as radio refractivity N , with N defined as follows:

$$N = (n - 1) \times 10^6 = \frac{77.6}{T} \times \left(P + \frac{4810e}{T} \right) \tag{3}$$

Under atmospheric duct conditions, electromagnetic wave propagation is refracted toward the surface of Earth and gets captured in a layer. Modified refractivity (M) is often applied to estimate these conditions. M is described by the following:

$$M(z) = N + \frac{z}{r_e 10^{-6}} \approx N + 0.157z \tag{4}$$

where r_e (m) represents the radius of the Earth and z (m) represents the height. In areas with a negative M vertical slope, electromagnetic waves are refracted toward the Earth’s surface and may get captured in an atmospheric duct.

Figure 4 shows the different types of atmospheric ducts, including a surface duct (Figure 4a), a surface-based duct (Figure 4b), an elevated duct (Figure 4c), and an evaporation duct (Figure 4d), and their parameters. In this paper, surface ducts and surface-based ducts are the targets of analysis.

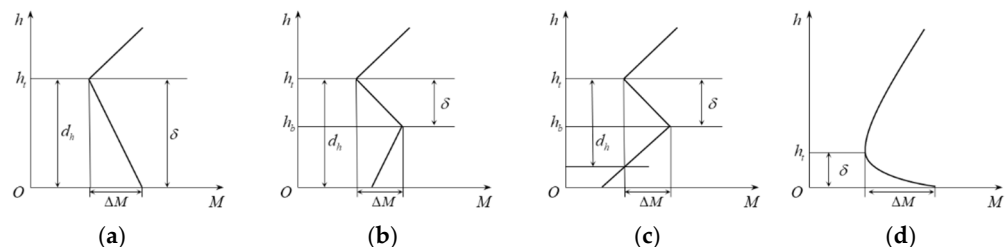


Figure 4. Different types of atmospheric duct: (a) Surface duct. (b) Surface-based duct. (c) Elevated duct. (d) Evaporation duct.

Atmospheric ducts such as surface ducts and elevated ducts can be determined from the modified refractivity profile in Equations (2)–(4). Radiosonde sounding data are used to calculate surface duct and elevated duct distributions.

The vertical resolution of the sounding data is inadequate to capture evaporation ducting events, since the altitude of an evaporation duct is often less than 40 m. The EDH specifies the evaporation duct’s ability to capture electromagnetic waves. As height increases, M decreases. The height at which M reaches its minimum value is defined as the EDH. In the paper, an evaporation duct model is applied to compute EDH distributions using the NCEP CFSv2 data. Several models relying on the Monin–Obukhov similarity theory, such as the Paulus–Jeske model [36], the Musson–Gauthier–Bruth model [37], the Liu–Katsaros–Businger model [38], the Babin–Young–Carton model [39], and NAVSLaM [40], have been developed to calculate evaporation duct distribution.

The NAVSLaM model utilizes the principles of the MOS and LKB theories, and incorporates air temperature, atmospheric pressure, wind speed, relative humidity at known altitudes, and average sea surface temperature to derive M -profiles.

To calculate the *M*-profiles, the NAVSLaM model requires profiles of temperature, pressure, and the partial pressure of water vapor. These profiles are obtained using the following equations:

$$T(z) = T(z_{0\theta}) + \frac{\theta_*}{\kappa} \left[\ln\left(\frac{z}{z_{0\theta}}\right) - \psi_h\left(\frac{z}{L}\right) \right] - \Gamma_d \tag{5}$$

$$q(z) = q(z_{0q}) + \frac{q_*}{\kappa} \left[\ln\left(\frac{z}{z_{0q}}\right) - \psi_h\left(\frac{z}{L}\right) \right] \tag{6}$$

$$p(z_2) = p(z_1) \exp\left(\frac{g(z_1 - z_2)}{RT_v}\right) \tag{7}$$

$$e = \frac{qp}{\varepsilon + (1 - \varepsilon)q} \tag{8}$$

where $T(z)$ and $q(z)$ are the air temperature and specific humidity at height z . $z_{0\theta}$ and z_{0q} are integration constants defining the temperature and specific humidity roughness length, respectively. θ_* and q_* represent the Monin-Obukhov temperature and specific humidity scaling parameters. The values of $z_{0\theta}$, z_{0q} , θ_* and q_* are computed using the TOGA COARE 3.0 bulk flux algorithm. κ represents von Karman’s constant. Γ_d represents the adiabatic lapse rate. L represents the Obukhov length. ψ_h is the temperature function. g , R , and ε correspond to gravity acceleration, the gas constant for dry air and the constant value of 0.622, respectively. T_v denotes the average value of virtual temperature at height of z_1 and z_2 .

This research used NAVSLaM to assess the distribution of evaporation ducts. The accuracy of NAVSLaM has been validated using radiosonde data, and is considered to be ideal for calculating the EDH [22,41]. Figure 5 shows the *M*-profiles calculated using NAVSLaM with an air temperature of 25 °C, a sea-surface temperature of 25 °C, a wind speed of 10 m s⁻¹, relative humidity of 80%, and air pressure of 1022.2 hPa. The calculated EDH is 13.7 m.

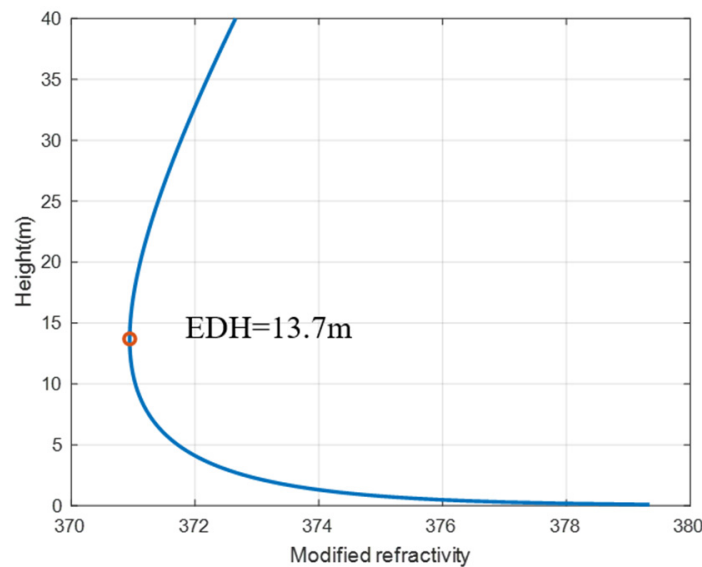


Figure 5. Modified refractivity profile estimated using the evaporation duct model.

2.3. Electromagnetic Wave Propagation Model

The PE model is used in this paper to simulate atmospheric duct effects on electromagnetic wave propagation. The standard PE can be derived from the Helmholtz equation [42]:

$$\frac{\partial^2 u(x, z)}{\partial z^2} + 2ik_0 \frac{\partial u(x, z)}{\partial x} + k_0^2 [M^2(x, z) - 1] u(x, z) = 0 \tag{9}$$

where x is the propagation range, z is the height, k_0 represents the number of free-space waves, M stands for the modified refractivity, and u represents the scalar part of the electric field given by:

$$u(x, z)e^{-ikx} = \psi(x, z) \tag{10}$$

where ψ is the electric or magnetic field.

Substituting the reduced function in the Helmholtz wave equation results in:

$$\frac{\partial^2 u}{\partial x^2} + \frac{\partial^2 u}{\partial z^2} + 2jk_0 \frac{\partial u}{\partial x} + k_0^2 (n^2 - 1)u = 0 \tag{11}$$

The field u in range x_{k+1} and at height z can be described by the Fourier split-step solution of the PE as follows:

$$u(x_{k+1}, z) = \exp\left(i\frac{k_0}{2}(M^2(x_k, z) - 1)\delta x\right) \times F^{-1}\left\{\exp\left(-i\frac{p^2\delta x}{2k_0}\right)F\{u(x_k, z)\}\right\} \tag{12}$$

where $F[\cdot]$ and $F^{-1}[\cdot]$ represent the Fourier transform and the Fourier inverse transform, respectively, δx represents the increment of range, and p represents the transform variable. The Fourier split-step PE solution is described in more detail in Refs. [43,44].

In this research, the APM is applied to compute the propagation of electromagnetic waves in a hybrid atmospheric duct. The APM is a hybrid model that combines the terrain parabolic equation model (TPEM) and the RPO model in relatively fast code. The APM has been extensively applied and evaluated in a variety of duct environments [24,31,32].

3. Statistical Analysis of Hybrid Atmospheric Ducts in the Northern South China Sea

3.1. Statistical Analysis of Surface Ducts and Elevated Ducts

This section uses sounding data from 2019 to 2020 to analyze the statistical characteristics of surface ducts and elevated ducts in the northern South China Sea. It is noted that as the minimum height of the sounding data at this sounding station is 66 m, the profile structure of atmospheric ducts below 66 m cannot be accurately obtained. This section includes only the occurrence probability of atmospheric ducts with a duct layer height greater than 66 m. Therefore, the probability result for the occurrence of surface ducts may be lower than the actual value. The statistical results in this section are used as a reference for the selection of simulation parameters in the next section. Table 2 shows the occurrence probability of surface ducts and elevated ducts, and Table 3 displays the statistical results for the characteristic parameters of elevated ducts. Figure 6 displays the average number of times surface ducts and elevated ducts appear each month.

Table 2. Occurrence probability of surface ducts and elevated ducts.

| Year | Sample Number | Surface Duct | Elevated Duct | Elevated or Surface Duct |
|------|---------------|--------------|---------------|--------------------------|
| 2019 | 726 | 15.01% | 74.52% | 79.06% |
| 2020 | 726 | 19.97% | 70.94% | 78.37% |

Table 3. Characteristic parameter distribution of elevated ducts.

| Year | h_t/m | h_b/m | δ/m | $\Delta M/M$ -Units |
|------|---------|---------|------------|---------------------|
| 2019 | 2023 | 1952.7 | 70.3 | 5.9 |
| 2020 | 1931 | 1861.2 | 69.8 | 6.18 |

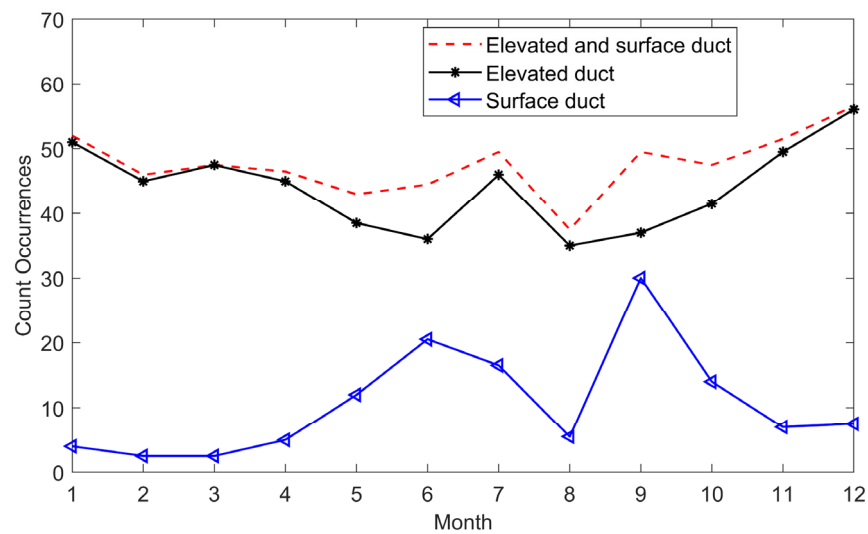


Figure 6. Monthly occurrences of surface ducts and elevated ducts.

As can be seen from Table 2, the occurrence probability of a surface duct is much lower than that of an elevated duct. The occurrence probability of a surface duct is about 20%, that of an elevated duct is about 70%, and that of an atmospheric duct is close to 80%. As can be seen from Table 3, the elevated ducts generally occur at about 2000 m, the thickness of the duct layer is about 70 m, and the duct strength is about 6 M. As can be seen from Figure 2, there are more occurrences of elevated ducts in January and December, more occurrences of surface ducts in June–September, and fewer occurrences of surface ducts in August, which may be due to the limitation of the minimum monitoring height of the station, resulting in low statistical results.

3.2. Statistical Analysis of Evaporation Ducts

This section uses the NCEP CFSv2 reanalysis data from 2019 to 2020 and NAVSLaM to analyze the statistical characteristics of evaporation ducts in the northern South China Sea. The monthly climatology of EDH distributions in the northern South China Sea is shown in Figure 7. The EDH distributions are uniform over the majority of the region. The mean EDH was low for the months of January to May, at less than 10 m with slight fluctuation. The EDH in the southeast of the study area was higher during January to May. When summer and autumn approached, the EDH increased rapidly. The average EDH was high in June to December (>10 m). The highest EDH was in October (around 15 m). Figure 8 shows the monthly averages and statistical features of the EDH. The average EDH was between 7 m and 10 m during January to May and started to increase from May, reaching a maximum of 14 m in October. In summary, evaporation ducts exist year-round in the study area, and the EDH is higher in summer and autumn.

3.3. Statistical Analysis of Hybrid Atmospheric Ducts in the Northern South China Sea

Figure 9 shows the statistical analysis of hybrid atmospheric ducts, which includes the count occurrences of elevated and surface ducts and the average EDH. Surface ducts and evaporation ducts show the same trends, both occurring frequently from June to December. As shown in Table 2, in 2019, the occurrence probability of surface ducts was 15.01% and that of elevated ducts was 74.52%. The occurrence probability of a surface duct or an elevated duct was 79.06%. Thus, the occurrence probability of a hybrid duct with a surface duct and an elevated duct was 10.47% in 2019. In addition, evaporation ducts exist in this sea area year-round, so hybrid ducts including an evaporation duct plus a surface duct or elevated duct appear more often during June to December.

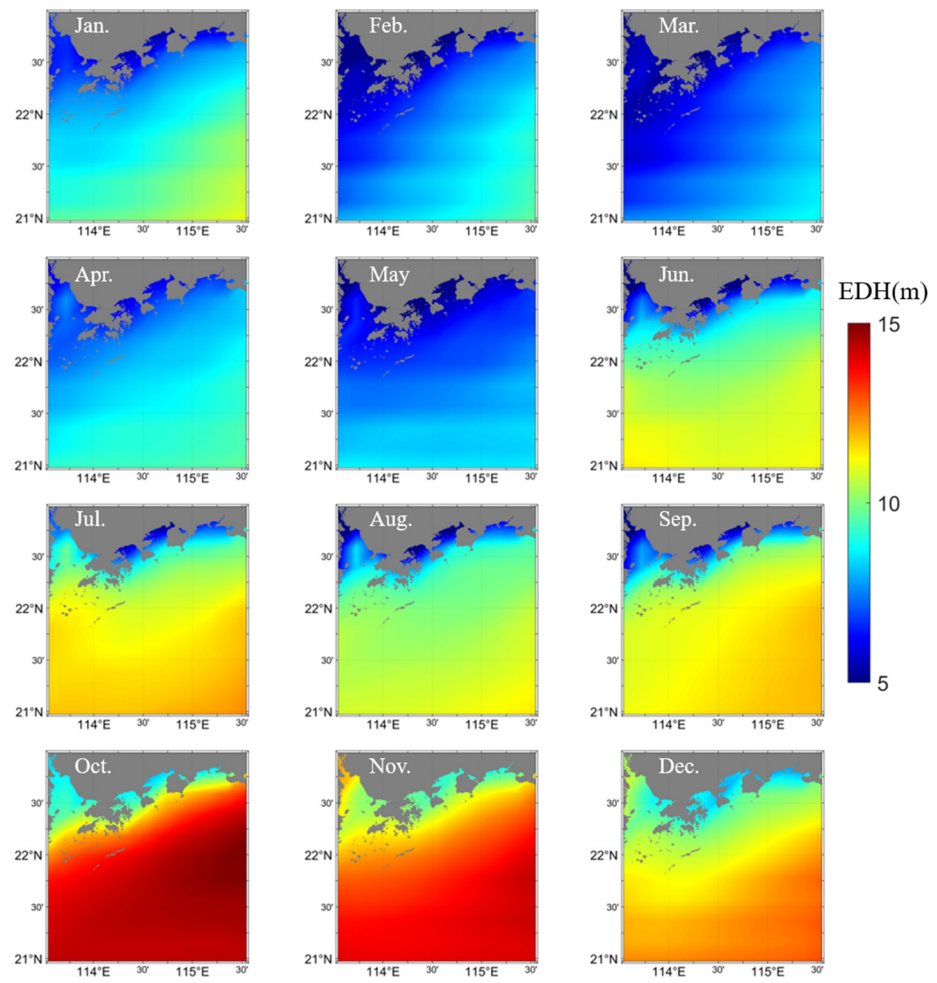


Figure 7. Spatiotemporal characteristics of the EDH in the study area.

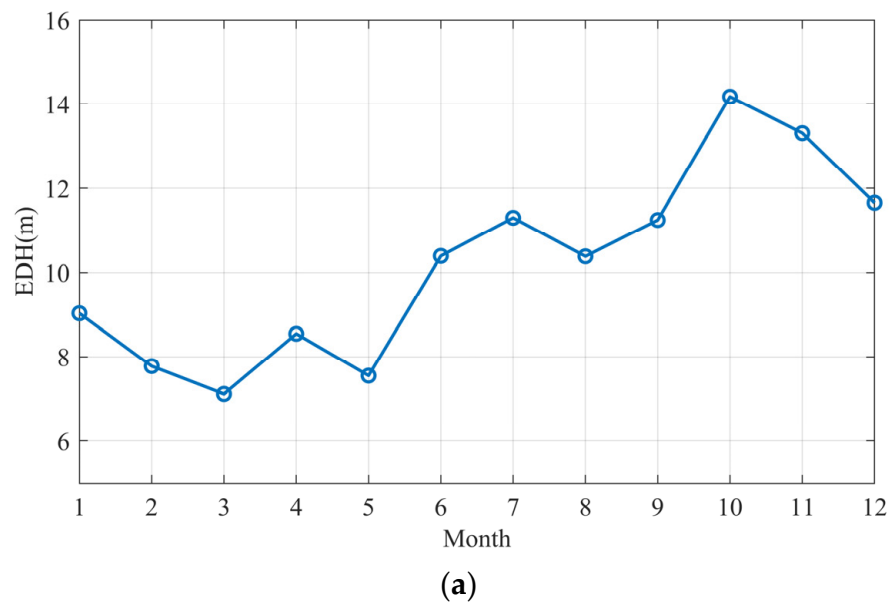


Figure 8. Cont.

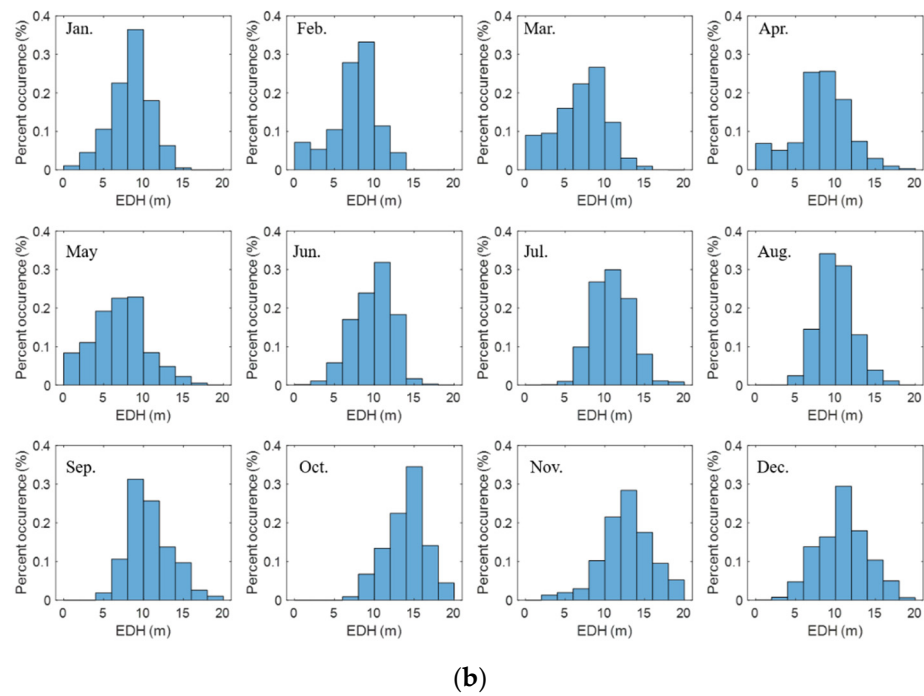


Figure 8. Monthly averages and statistical features of the EDH: (a) Monthly average of the EDH. (b) Percent occurrence of the EDH.

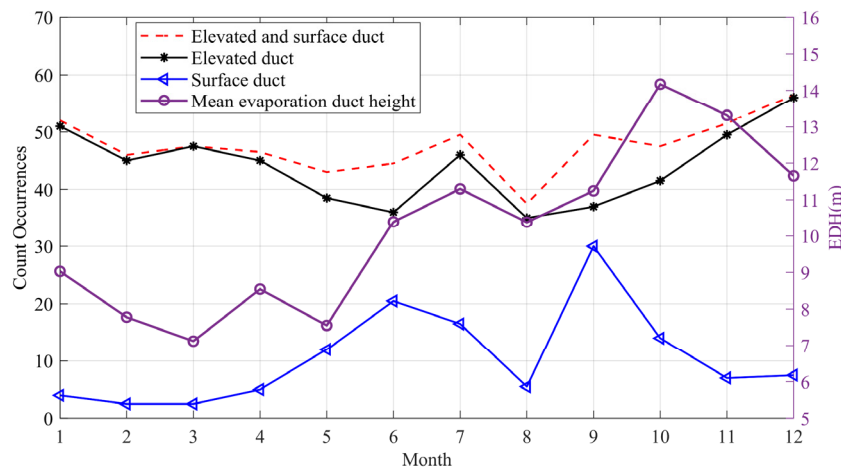


Figure 9. Statistical analysis of hybrid atmospheric ducts.

4. Influence of Hybrid Atmospheric Ducts on Over-the-Horizon Electromagnetic Wave Propagation

As demonstrated in Section 3.1, the average height of an elevated duct is roughly 2000 m, indicating that it has limited effect on microwave propagation at low height. In this section, the analysis focuses on the simulation and evaluation of the impact of surface ducts and evaporation ducts on microwave propagation characteristics near the sea surface.

A typical atmospheric duct environment is selected and divided into three situations: surface ducts, evaporation ducts, and hybrid ducts including surface ducts and evaporation ducts. The influence of each on microwave propagation near the ocean surface is studied. The bottom height of the surface duct is 40 m, the top height is 81 m, the duct strength is 7.8 M, and the duct layer thickness is 41 m. The EDH is 15 m and the duct strength is 11.2 M. The parameters for the APM model are presented in Table 4. Previous research [45] indicates that the optimal antenna height inside the evaporation channel is between 3 and 7 m. Therefore, we take an antenna height of 5 m as an example for analysis. The radio wave frequency is

8 GHz, and the propagation distance is 200 km. The different atmospheric duct profiles and simulated distributions of microwave propagation path loss with distance and height under the three conditions are shown in Figure 10.

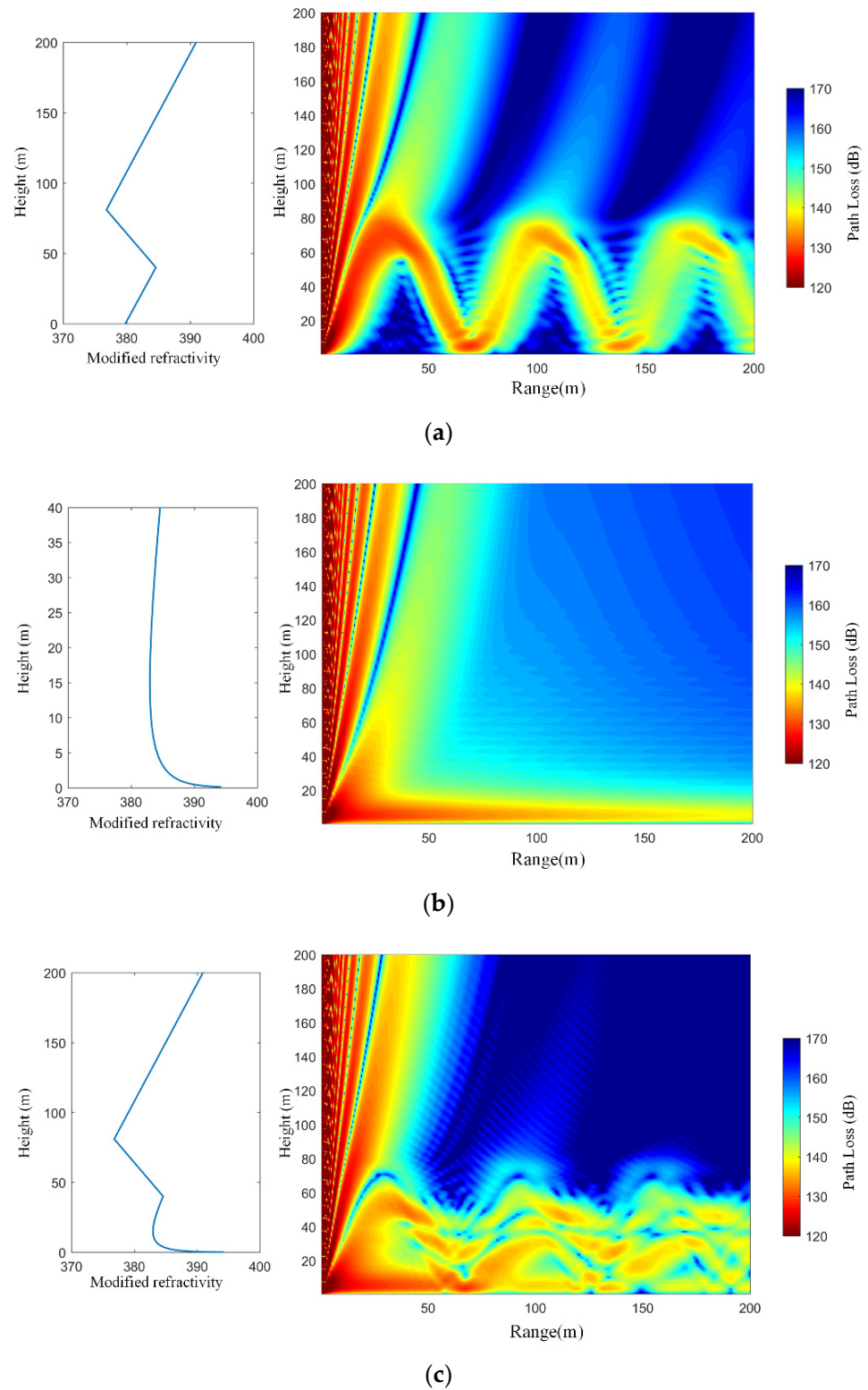


Figure 10. Modified refractivity profiles and path loss distributions in three cases: (a) surface duct; (b) evaporation duct; and (c) hybrid duct.

Table 4. Parameters for the PE model.

| Parameter | Value |
|-------------------------------|---|
| Transmitting antenna height | 5 m |
| Transmitting frequency | 8 GHz |
| Antenna type | Omni antenna |
| Polarization type | Horizontal |
| Height | 0–200 m |
| Range | 0–200 km |
| Modified refractivity profile | Surface duct/evaporation duct/hybrid duct |

It can be seen from Figure 10a that when only a surface duct exists, the microwave energy first propagates upwards, refracts downwards when it reaches the top of the surface duct layer at about 80 m, and then continues to refract upwards when it reaches the sea surface. The microwave energy is trapped in the surface duct layer and propagates forward beyond the visual range, and there is an obvious shadow zone in the microwave energy. Figure 10b shows the path loss distribution of the propagation of microwave in the evaporation duct environment. It can be seen that the microwave energy is captured in the evaporation duct layer and propagates forward, and the path loss in the area below the EDH is small. Figure 10c shows the distribution of path loss when a surface duct and an evaporation duct coexist. It can be seen that, compared with a surface duct alone, due to the capture effect of the evaporation duct on low-altitude electromagnetic waves, the shadow zone of path loss is made up, and only blind areas with a smaller spatial scale exist sporadically. Compared with an evaporation duct alone, the height range with smaller path loss expands upwards due to the capture effect of the surface duct on higher microwave energy. In summary, compared with a case in which only one atmospheric duct is considered, a hybrid duct structure containing two ducts can capture more microwave energy at a lower receiving height.

Figure 11 shows the variation in path loss with distance and altitude for the above three simulation situations. As shown in Figure 11a, when the receiving antenna height is 5 m, for the evaporation duct, the path loss increases gently with increasing propagation distance, and the path loss at 200 km is only about 139 dB, so the microwaves are trapped in the evaporation duct layer and propagate beyond the visual range. For the surface duct, the path loss fluctuates with increasing distance, reaching as high as 50 dB, and the fluctuation range is about 70 km. When the evaporation duct and the surface duct are considered together, the curve of path loss with distance is generally similar to that for only the evaporation duct, but it also begins to fluctuate beyond a propagation distance of 50 km, with a maximum fluctuation difference of about 15 dB. Figure 11b shows the change in path loss with receiving height at a propagation distance of 200 km. For the evaporation duct, the path loss first decreases with increasing receiving height, reaches a minimum of 138 dB at a receiving height of 3.5 m, and then increases with increasing receiving height. For the surface duct, the microwave energy at 200 km is concentrated at low receiving heights, so the path loss below 60 m is small, at about 140 dB. However, for the hybrid duct, the path loss is small at receiving heights below 60 m, but there are some fluctuations. The local minimum of the path loss is 139 dB at 5 m, but with increasing height, the path loss increases to a local maximum of 163 dB at 12 m, decreases with increasing height, and finally increases with receiving height above 60 m. Comparing the three cases, for the hybrid duct, the path loss at higher receiving heights is greater than that for the other two cases, that is, the microwave energy is more trapped at low receiving heights, but there are also fluctuations. The above conclusions provide a basis for evaluating the optimal antenna height of offshore electromagnetic systems in practical applications.

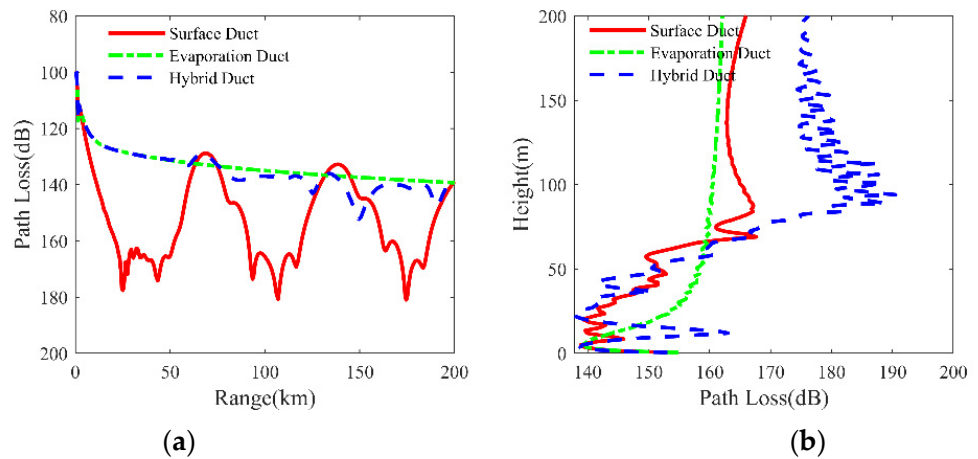


Figure 11. Path loss changes with distance and height: (a) at a receiving height of 5 m; and (b) at a receiving distance of 200 km.

5. Discussion

This section focuses on the effects of microwave frequency and antenna height on the path loss of microwave propagation in the three duct environments considered in this paper.

5.1. Influence of Frequency on Electromagnetic Wave Propagation in Hybrid Atmospheric Ducts

The three duct environments have different effects on electromagnetic wave propagation with different frequencies. Assuming that the radio wave frequency varies from 1 GHz to 20 GHz, other environmental parameters and emission information are identical to those in Table 4. Figure 12 shows path loss distributions for surface ducts with different frequencies. It can be seen that surface ducts have stronger trapping ability for low-frequency signals, while high-frequency signals exhibit significant shadowing in surface ducts. Figure 13 shows the path loss distributions for evaporation ducts with different frequencies. Unlike the surface ducts, the evaporation ducts have a stronger trapping effect on high-frequency signals. The 1 GHz signal can barely be trapped by evaporation ducts, while the energy of the 20 GHz signal is more concentrated in the duct layer. Figure 14 shows the path loss distributions for hybrid ducts with different frequencies. For a 1 GHz signal, the propagation in hybrid ducts is similar to that in surface ducts alone. However, for 8 GHz and 12 GHz signals, hybrid ducts including evaporation ducts fill in the shadow zone of the surface ducts where the electromagnetic energy is concentrated.

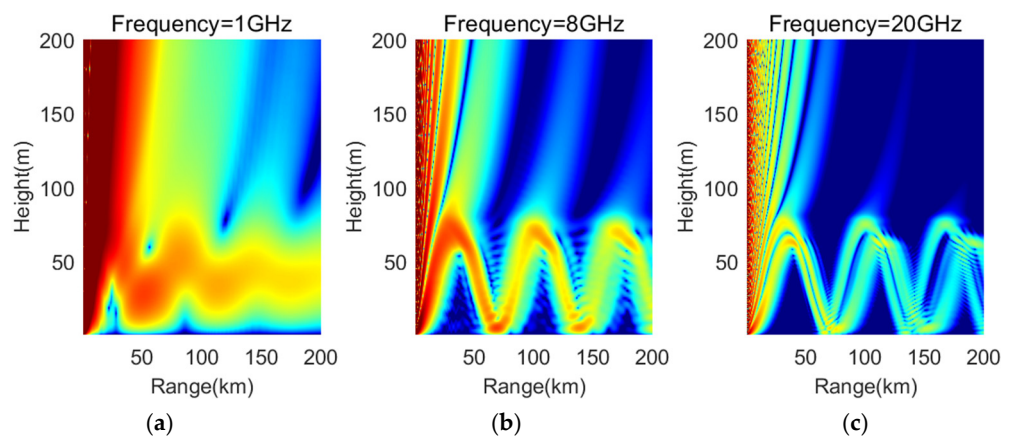


Figure 12. Path loss distributions for surface ducts with different frequencies: (a) frequency of 1 GHz, (b) frequency of 8 GHz, and (c) frequency of 20 GHz.

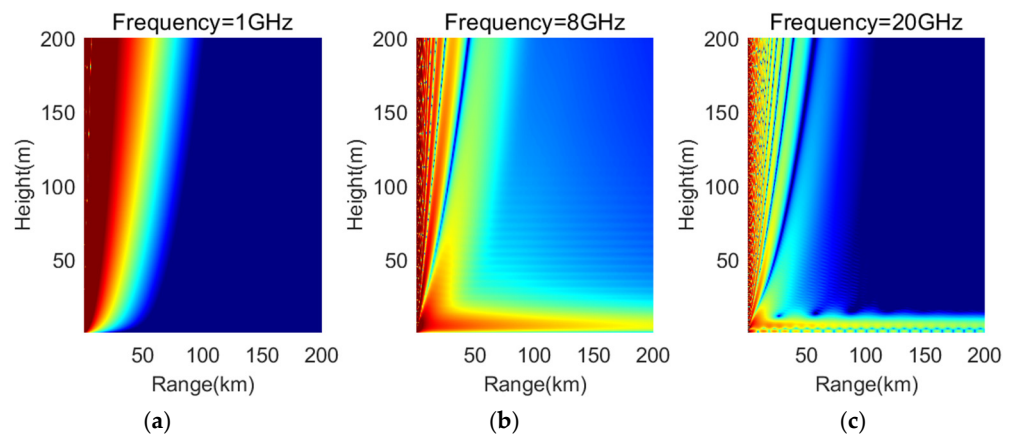


Figure 13. Path loss distributions for evaporation ducts with different frequencies: (a) frequency of 1 GHz, (b) frequency of 8 GHz, and (c) frequency of 20 GHz.

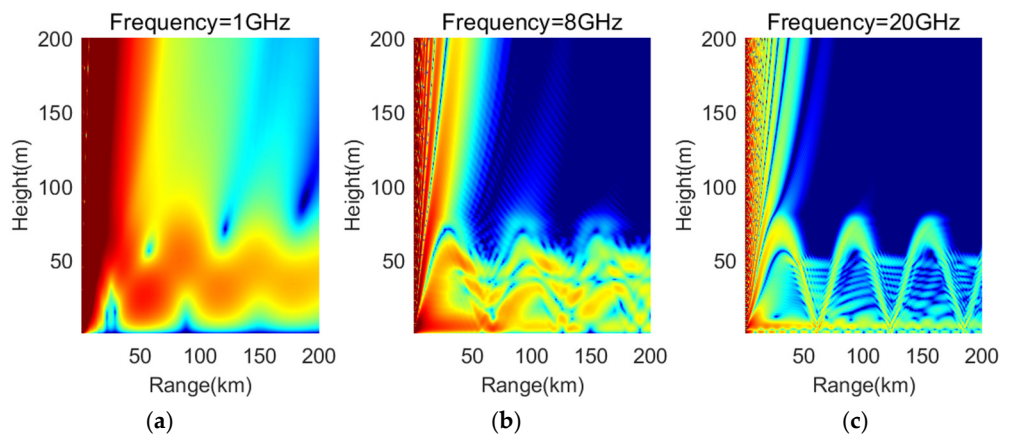


Figure 14. Path loss distributions for hybrid ducts with different frequencies: (a) frequency of 1 GHz, (b) frequency of 8 GHz, and (c) frequency of 20 GHz.

Figure 15 presents the path loss of electromagnetic waves with different frequencies when the receiving height is 5 m and the receiving distance is 200 km. When only evaporation ducts are considered, the channel has obvious frequency selectivity, and electromagnetic waves with a frequency of 7–20 GHz can be well captured in the evaporation duct layer with a path loss of about 140 dB. When only surface ducts are considered, electromagnetic waves with a frequency of 1–20 GHz can be well trapped, and the path loss ranges from 138 dB at a frequency of 5 GHz to 161 dB at a frequency of 15 GHz. Considering hybrid ducts, the microwave energy in the 1–20 GHz frequency band can all be well trapped, and the path loss fluctuates around 140 dB. In summary, compared with considering only one duct, when considering the interaction of surface ducts and evaporation ducts, the frequency selectivity of the channel is no longer obvious, and the microwave energy in the frequency band of 1–20 GHz can be captured by the duct layer, thus realizing over-the-horizon propagation.

5.2. Influence of Antenna Height on Electromagnetic Wave Propagation in Hybrid Atmospheric Ducts

The three duct environments have different effects on electromagnetic wave propagation at different antenna heights. Assuming that the transmitting antenna height is the same as the receiving antenna height and the antenna height is taken as 2–40 m, other environmental parameters are the same as those in Table 4. Figure 16 shows the path loss distributions for surface ducts with different antenna heights. For the simulated surface duct parameters, the electromagnetic energy with lower antenna heights (5 m) exhibits a larger shadow zone in surface ducts. For higher antenna heights (20 m, 40 m), the shadow

zone still exists but is smaller. Figure 17 shows the path loss distributions for evaporation ducts with different antenna heights. Evaporation ducts have stronger trapping ability for electromagnetic waves with an antenna height of 5 m. Figure 18 shows the path loss distributions for hybrid ducts with different antenna heights. It can be seen that due to the presence of evaporation ducts, the shadow zone of the electromagnetic energy is filled, as compared to having only surface ducts. Moreover, for a 40 m antenna height, since the bottom height of the surface duct is also at 40 m, the electromagnetic energy is more concentrated at this height.

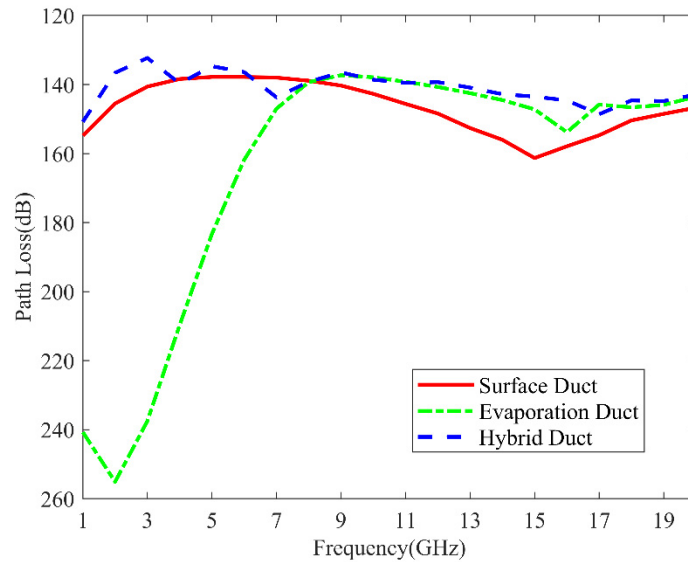


Figure 15. Microwave propagation path loss at different frequencies with a receiving height of 5 m and a receiving distance of 200 km.

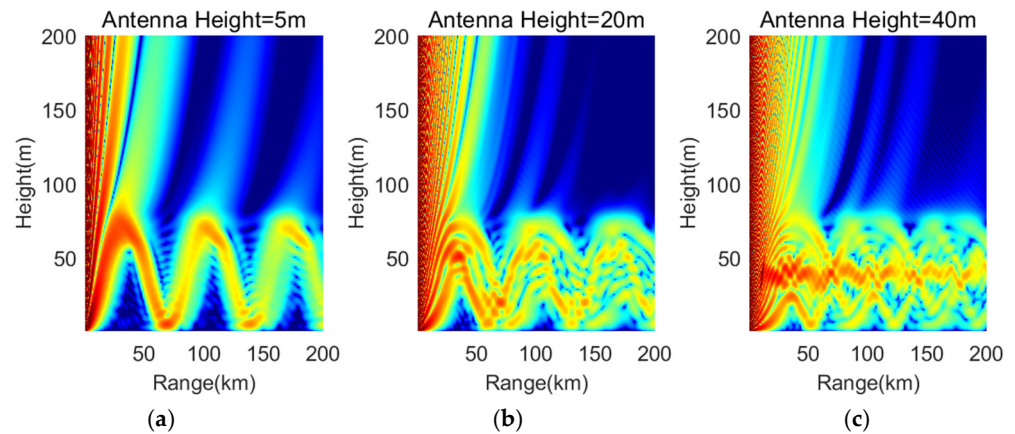


Figure 16. Path loss distributions for surface ducts with different antenna heights: (a) antenna height of 1 m, (b) antenna height of 20 m, and (c) antenna height of 40 m.

Figure 19 shows the path loss of electromagnetic waves with different antenna heights. When only evaporation ducts are considered, the path loss is small when the antenna height is low, and the path loss is the smallest when the antenna height is 5 m, at 139.3 dB. With increasing antenna height, microwaves do not transmit in the evaporation duct layer, and the path loss is large. When considering only surface ducts, the path loss decreases to 138.9 dB at an antenna height of 5 m, increases to 157.9 dB at an antenna height of 10 m, and then decreases to about 138 dB. The microwave path loss is not affected by the antenna height, and the main reason the path loss is larger at an antenna height of 10 m is that the receiving antenna is in the energy blind area. When hybrid ducts are considered, the

path loss of microwave propagation is less affected by the antenna height, and basically fluctuates between 140 dB and 150 dB.

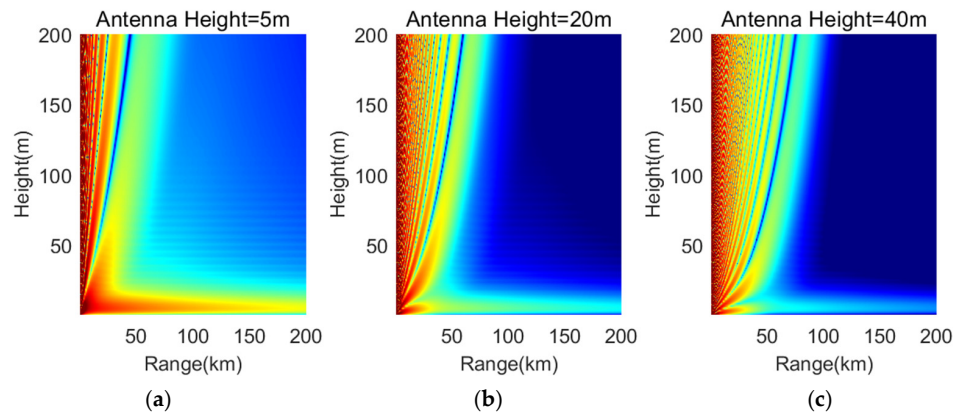


Figure 17. Path loss distributions for evaporation ducts with different antenna heights: (a) antenna height of 1 m, (b) antenna height of 20 m, and (c) antenna height of 40 m.

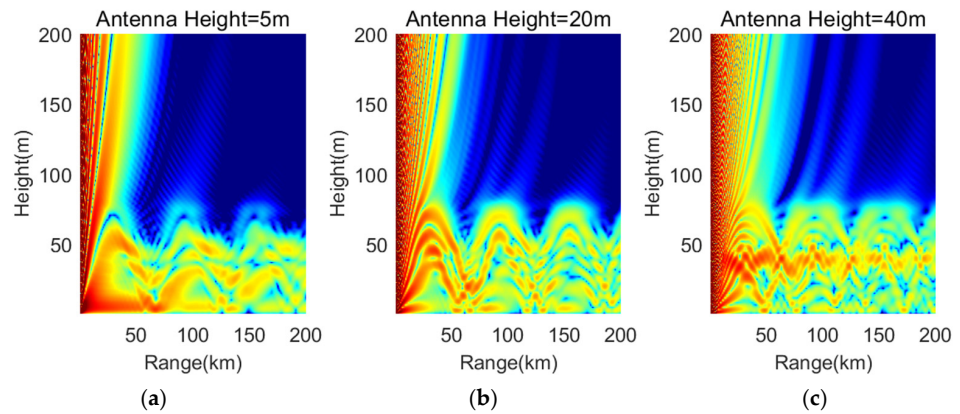


Figure 18. Path loss distributions for hybrid ducts with different antenna heights: (a) antenna height of 1 m, (b) antenna height of 20 m, and (c) antenna height of 40 m.

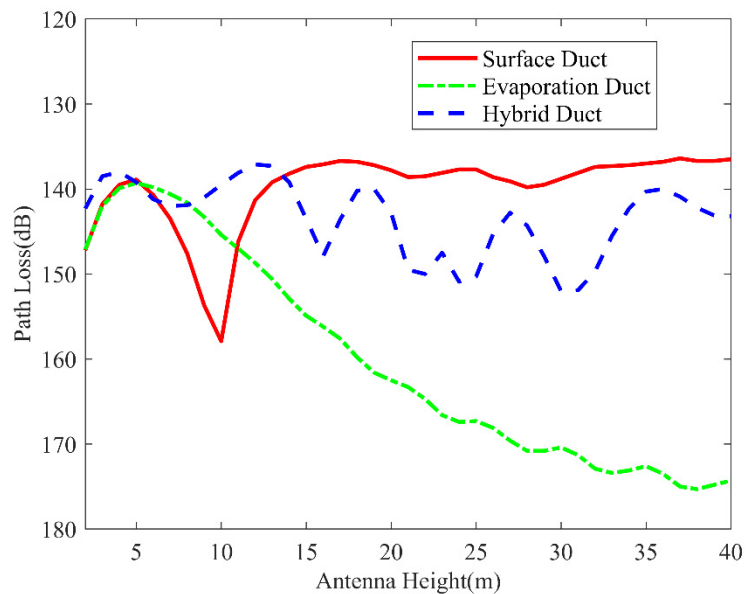


Figure 19. Path loss of microwave propagation at different antenna heights with a frequency of 8 GHz and a receiving distance of 200 km.

In summary, microwave propagation characteristics are greatly influenced by microwave frequency and antenna height when only evaporation ducts are considered, whereas when surface ducts appear, the microwave propagation characteristics near the sea surface are less influenced by the microwave frequency and antenna height if the interaction of the two ducts is considered.

6. Conclusions

In this paper, the statistical features of hybrid atmospheric ducts are investigated using long-term radiosonde sounding data and reanalysis data for the northern South China Sea. The effects of a hybrid duct profile including evaporation ducts and surface ducts on radio wave propagation near the ocean surface are presented. The subsequent conclusions are obtained.

- (1) The statistical features of hybrid atmospheric ducts in the northern South China Sea are analyzed. It is found that the occurrence probability of elevated ducts is about 70% and that of surface ducts is about 20%. Evaporation ducts are nearly permanent in this sea area, and hybrid ducts including evaporation ducts and surface ducts or elevated ducts occur more often during June to December.
- (2) The influence of hybrid ducts on radio wave propagation near the ocean surface is simulated. When considering hybrid ducts compared with surface ducts alone, the blind area of microwave energy at low height is compensated. Compared with evaporation ducts alone, more microwave energy can be captured at a lower receiving height. The path loss begins to fluctuate beyond a propagation distance of 50 km with a maximum fluctuation of 15 dB when hybrid ducts exist. The electromagnetic wave energy is more trapped at lower propagation height.
- (3) The influence of different electromagnetic wave frequencies and antenna heights on electromagnetic wave propagation for hybrid ducts is discussed. Microwave propagation characteristics near the sea surface are less influenced by microwave frequency and antenna height when hybrid ducts exist.

In the future, it could be useful to conduct further simulation studies to evaluate the impacts of local atmospheric anomalies on electromagnetic wave propagation over atmospheric ducts. Factors such as temperature, humidity, and wind speed gradients may create additional refractive index structures that can affect the propagation characteristics of EM waves. Additionally, the results of this research could be further validated through field experiments. The findings of this research can potentially be applied in other regions with similar oceanic conditions, but caution should be taken, as findings may differ based on location and season.

Author Contributions: Conceptualization, Y.S. and S.W.; methodology, Y.S.; software, S.W.; validation, S.W., F.Y. and K.Y.; formal analysis, F.Y.; investigation, Y.S.; resources, Y.S.; data curation, Y.S.; writing—original draft preparation, Y.S.; writing—review and editing, S.W.; visualization, Y.S.; supervision, K.Y.; project administration, K.Y.; funding acquisition, Y.S. and K.Y. All authors have read and agreed to the published version of the manuscript.

Funding: This research was funded by: the National Natural Science Foundation of China, grant number 42076198, 41906160 and 42176190; the Innovation Capability Support Program of Shaanxi, grant number 2022KJXX-76; the Fundamental Research Funds for the Central Universities, grant number 3102021HHZY030010; and Innovation Foundation for Doctor Dissertation of Northwestern Polytechnical University, grant number CX2022008.

Institutional Review Board Statement: Not applicable.

Informed Consent Statement: Not applicable.

Data Availability Statement: Sounding data: <http://weather.uwyo.edu/upperair/sounding.html>, accessed on 4 January 2023; NCEP CFSv2 data: <https://rda.ucar.edu>, accessed on 5 January 2023.

Acknowledgments: We thank all the editors and reviewers for their valuable comments, which greatly improved the presentation of this paper.

Conflicts of Interest: The authors declare no conflict of interest.

References

- Zhao, X.; Wang, D.; Huang, S.; Huang, K.; Chen, J. Statistical Estimations of Atmospheric Duct over the South China Sea and the Tropical Eastern Indian Ocean. *Chin. Sci. Bull.* **2013**, *58*, 2794–2797. [[CrossRef](#)]
- Huang, L.; Zhao, X.; Liu, Y. The Statistical Characteristics of Atmospheric Ducts Observed Over Stations in Different Regions of American Mainland Based on High-Resolution GPS Radiosonde Soundings. *Front. Environ. Sci.* **2022**, *10*, 946226. [[CrossRef](#)]
- Pastore, D.M.; Greenway, D.P.; Stanek, M.J.; Wessinger, S.E.; Haack, T.; Wang, Q.; Hackett, E.E. Comparison of Atmospheric Refractivity Estimation Methods and Their Influence on Radar Propagation Predictions. *Radio Sci.* **2021**, *56*, e2020RS007244. [[CrossRef](#)]
- Huang, L.-F.; Liu, C.-G.; Wang, H.-G.; Zhu, Q.-L.; Zhang, L.-J.; Han, J.; Zhang, Y.-S.; Wang, Q.-N. Experimental Analysis of Atmospheric Ducts and Navigation Radar Over-the-Horizon Detection. *Remote Sens.* **2022**, *14*, 2588. [[CrossRef](#)]
- Wang, S.; Yang, K.; Shi, Y.; Zhang, H.; Yang, F.; Hu, D.; Dong, G.; Shu, Y. Long-Term over-the-Horizon Microwave Channel Measurements and Statistical Analysis in Evaporation Ducts over the Yellow Sea. *Front. Mar. Sci.* **2023**, *10*, 1077470. [[CrossRef](#)]
- Yang, C.; Wang, J.; Ma, J. Exploration of X-Band Communication for Maritime Applications in the South China Sea. *Antennas Wirel. Propag. Lett.* **2022**, *21*, 481–485. [[CrossRef](#)]
- Yang, C.; Wang, J. The Investigation of Cooperation Diversity for Communication Exploiting Evaporation Ducts in the South China Sea. *IEEE Trans. Antennas Propag.* **2022**, *70*, 8337–8347. [[CrossRef](#)]
- Xu, L.; Yardim, C.; Mukherjee, S.; Burkholder, R.J.; Wang, Q.; Fernando, H.J.S. Frequency Diversity in Electromagnetic Remote Sensing of Lower Atmospheric Refractivity. *IEEE Trans. Antennas Propag.* **2022**, *70*, 547–558. [[CrossRef](#)]
- Robinson, L.; Newe, T.; Burke, J.; Toal, D. A Simulated and Experimental Analysis of Evaporation Duct Effects on Microwave Communications in the Irish Sea. *IEEE Trans. Antennas Propag.* **2022**, *70*, 4728–4737. [[CrossRef](#)]
- Ma, J.; Wang, J.; Yang, C. Long-Range Microwave Links Guided by Evaporation Ducts. *IEEE Commun. Mag.* **2022**, *60*, 68–72. [[CrossRef](#)]
- Zhang, Q.; Wang, S.; Shi, Y.; Yang, K. Measurements and Analysis of Maritime Wireless Channel at 8GHz in the South China Sea Region. *IEEE Trans. Antennas Propag.* **2023**, *71*, 2674–2681. [[CrossRef](#)]
- Zhou, Y.; Liu, Y.; Qiao, J.; Li, J.; Zhou, C. Statistical Analysis of the Spatiotemporal Distribution of Lower Atmospheric Ducts over the Seas Adjacent to China, Based on the ECMWF Reanalysis Dataset. *Remote Sens.* **2022**, *14*, 4864. [[CrossRef](#)]
- Yang Kun-De; Ma Yuan-Liang; Shi Yang Spatio-temporal distributions of evaporation duct for the West Pacific Ocean. *Acta Phys. Sin.* **2009**, *58*, 7339–7350. [[CrossRef](#)]
- Zhao, X.; Yang, P.; Zhou, F.; Zhou, Z. Comparison of Evaporation Duct Height Statistics Based on Surface Bulk Measurements over Yongxing Island. *Antennas Wirel. Propag. Lett.* **2023**, 1–5. [[CrossRef](#)]
- Huang, L.; Zhao, X.; Liu, Y.; Yang, P.; Ding, J.; Zhou, Z. The Diurnal Variation of the Evaporation Duct Height and Its Relationship with Environmental Variables in the South China Sea. *IEEE Trans. Antennas Propag.* **2022**, *70*, 10865–10875. [[CrossRef](#)]
- Yang, C.; Shi, Y.; Wang, J.; Feng, F. Regional Spatiotemporal Statistical Database of Evaporation Ducts Over the South China Sea for Future Long-Range Radio Application. *IEEE J. Sel. Top. Appl. Earth Obs. Remote Sens.* **2022**, *15*, 6432–6444. [[CrossRef](#)]
- Zhang, Q.; Yang, K.; Shi, Y. Spatial and Temporal Variability of the Evaporation Duct in the Gulf of Aden. *Tellus A: Dyn. Meteorol. Oceanogr.* **2016**, *68*, 29792. [[CrossRef](#)]
- Yang, K.; Zhang, Q.; Shi, Y.; He, Z.; Lei, B.; Han, Y. On Analyzing Space-Time Distribution of Evaporation Duct Height over the Global Ocean. *Acta Oceanol. Sin.* **2016**, *35*, 20–29. [[CrossRef](#)]
- Yang, C.; Shi, Y.; Wang, J. The Preliminary Investigation of Communication Characteristics Using Evaporation Duct across the Taiwan Strait. *JMSE* **2022**, *10*, 1493. [[CrossRef](#)]
- Qiu, Z.; Zhang, C.; Wang, B.; Hu, T.; Zou, J.; Li, Z.; Chen, S.; Wu, S. Analysis of the Accuracy of Using ERA5 Reanalysis Data for Diagnosis of Evaporation Ducts in the East China Sea. *Front. Mar. Sci.* **2023**, *9*, 1108600. [[CrossRef](#)]
- Han, J.; Wu, J.-J.; Zhu, Q.-L.; Wang, H.-G.; Zhou, Y.-F.; Jiang, M.-B.; Zhang, S.-B.; Wang, B. Evaporation Duct Height Nowcasting in China's Yellow Sea Based on Deep Learning. *Remote Sens.* **2021**, *13*, 1577. [[CrossRef](#)]
- Wang, Q.; Burkholder, R.J.; Yardim, C.; Wang, Q.; Yamaguchi, R.; Franklyn, K.; Ortiz-Suslow, D.; Creagan, E.; Fernando, J. Estimation of Evaporation Duct and Surface-Based Duct Parameters from a Combined Refractivity Model. In Proceedings of the 2018 IEEE International Symposium on Antennas and Propagation & USNC/URSI National Radio Science Meeting, Boston, MA, USA, 8–13 July 2018; pp. 879–880.
- Ozgun, O.; Sahin, V.; Erguden, M.E.; Apaydin, G.; Yilmaz, A.E.; Kuzuoglu, M.; Sevgi, L. PETOOL v2.0: Parabolic Equation Toolbox with Evaporation Duct Models and Real Environment Data. *Comput. Phys. Commun.* **2020**, *256*, 107454. [[CrossRef](#)]
- Barrios, A.; Patterson, W.; Sprague, R. *Advanced Propagation Model (APM) Version 2.1.04 Computer Software Configuration Item (CSCI) Documents*; Space and Naval Warfare Systems Center: San Diego, CA, USA, 2002.

25. Anderson, K.; Brooks, B.; Caffrey, P.; Clarke, A.; Cohen, L.; Crahan, K.; Davidson, K.; De Jong, A.; De Leeuw, G.; Dion, D.; et al. The RED Experiment: An Assessment of Boundary Layer Effects in a Trade Winds Regime on Microwave and Infrared Propagation over the Sea. *Bull. Amer. Meteor. Soc.* **2004**, *85*, 1355–1366. [[CrossRef](#)]
26. Wang, Q.; Alappatt, D.P.; Billingsley, S.; Blomquist, B.; Burkholder, R.J.; Christman, A.J.; Creegan, E.D.; De Paolo, T.; Eleuterio, D.P.; Fernando, H.J.S.; et al. CASPER: Coupled Air-Sea Processes and Electromagnetic Ducting Research. *Bull. Amer. Meteorol. Soc.* **2018**, *99*, 1449–1471. [[CrossRef](#)]
27. Wang, Q.; Burkholder, R.J.; Yardim, C.; Xu, L.; Pozderac, J.; Christman, A.; Fernando, H.J.S.; Alappattu, D.P.; Wang, Q. Range and Height Measurement of X-Band EM Propagation in the Marine Atmospheric Boundary Layer. *IEEE Trans. Antennas Propag.* **2019**, *67*, 2063–2073. [[CrossRef](#)]
28. Wang, S.; Yang, K.; Shi, Y.; Yang, F.; Zhang, H. Impact of Evaporation Duct on Electromagnetic Wave Propagation During a Typhoon. *J. Ocean Univ. China* **2022**, *21*, 1069–1083. [[CrossRef](#)]
29. Wang, S.; Yang, K.; Shi, Y.; Yang, F. Observations of Anomalous Over-the-Horizon Propagation in the Evaporation Duct Induced by Typhoon Kompasu (202118). *Antennas Wirel. Propag. Lett.* **2022**, *21*, 963–967. [[CrossRef](#)]
30. Yang, F.; Yang, K.; Shi, Y.; Wang, S.; Zhang, H.; Zhao, Y. The Effects of Rainfall on Over-the-Horizon Propagation in the Evaporation Duct over the South China Sea. *Remote Sens.* **2022**, *14*, 4787. [[CrossRef](#)]
31. Shi, Y.; Kun-De, Y.; Yang, Y.-X.; Ma, Y.-L. Influence of Obstacle on Electromagnetic Wave Propagation in Evaporation Duct with Experiment Verification. *Chin. Phys. B* **2015**, *24*, 054101. [[CrossRef](#)]
32. Shi, Y.; Yang, K.-D.; Yang, Y.-X.; Ma, Y.-L. Experimental Verification of Effect of Horizontal Inhomogeneity of Evaporation Duct on Electromagnetic Wave Propagation. *Chin. Phys. B* **2015**, *24*, 044102. [[CrossRef](#)]
33. Lin, J.; Qing-hong, L.; Yong-gang, Z. Diagnosis of the Inhomogeneous Evaporation Duct and Its Effects on the Electromagnetic Wave Propagation of the Radar. In Proceedings of the 2019 Cross Strait Quad-Regional Radio Science and Wireless Technology Conference (CSQRWC), Taiyuan, China, 18–21 July 2019; pp. 1–3.
34. University of Wyoming Sounding Map. Available online: <http://weather.uwyo.edu/upperair/seasia.html> (accessed on 4 January 2023).
35. Saha, S.; Moorthi, S.; Wu, X.; Wang, J.; Nadiga, S.; Tripp, P.; Behringer, D.; Hou, Y.-T.; Chuang, H.; Iredell, M.; et al. The NCEP Climate Forecast System Version 2. *J. Clim.* **2014**, *27*, 2185–2208. [[CrossRef](#)]
36. Paulus, R.A. Practical Application of an Evaporation Duct Model. *Radio Sci.* **1985**, *20*, 887–896. [[CrossRef](#)]
37. Musson-Genon, L.; Gauthier, S.; Bruth, E. A Simple Method to Determine Evaporation Duct Height in the Sea Surface Boundary Layer. *Radio Sci.* **1992**, *27*, 635–644. [[CrossRef](#)]
38. Liu, W.T.; Katsaros, K.B.; Businger, J.A. Bulk Parameterization of Air-Sea Exchanges of Heat and Water Vapor Including the Molecular Constraints at the Interface. *J. Atmos. Sci.* **1979**, *36*, 1722–1735. [[CrossRef](#)]
39. Babin, S.M.; Young, G.S.; Carton, J.A. A New Model of the Oceanic Evaporation Duct. *J. Appl. Meteor.* **1997**, *36*, 193–204. [[CrossRef](#)]
40. Frederickson, P.A. Further Improvements and Validation for the Navy Atmospheric Vertical Surface Layer Model (NAVSLaM). In Proceedings of the 2015 USNC-URSI Radio Science Meeting (Joint with AP-S Symposium), Vancouver, BC, Canada, 19–24 July 2015; p. 242.
41. Babin, S.M.; Dockery, G.D. LKB-Based Evaporation Duct Model Comparison with Buoy Data. *J. Appl. Meteor.* **2002**, *41*, 434–446. [[CrossRef](#)]
42. Kraut, S.; Anderson, R.H.; Krolik, J.L. A Generalized Karhunen–Loeve Basis for Efficient Estimation of Tropospheric Refractivity Using Radar Clutter. *IEEE Trans. Signal Process.* **2004**, *52*, 48–60. [[CrossRef](#)]
43. Goldhirsh, J.; Dockery, D. Propagation Factor Errors Due to the Assumption of Lateral Homogeneity. *Radio Sci.* **1998**, *33*, 239–249. [[CrossRef](#)]
44. Derksen, J. Radar Performance Modelling; A Study of Radar Performance Assessment Accuracy to the Resolution of Atmospheric Input Data. Master’s Thesis, Delft University of Technology, Delft, The Netherlands, 2016.
45. Wang, S.; Han, J.; Shi, Y.; Yang, K.; Huang, C.; Yang, F. The Influence of Antenna Height on Microwave Propagation in Evaporation Duct. In Proceedings of the Global Oceans 2020: Singapore—U.S. Gulf Coast, Virtual, 5–14 October 2020; pp. 1–5.

Disclaimer/Publisher’s Note: The statements, opinions and data contained in all publications are solely those of the individual author(s) and contributor(s) and not of MDPI and/or the editor(s). MDPI and/or the editor(s) disclaim responsibility for any injury to people or property resulting from any ideas, methods, instructions or products referred to in the content.